Polymer Bulletin (2019) 76:1239–1256
https://doi.org/10.1007/s00289-018-2418-7

ORIGINAL PAPER

Agarose-coated Fe_3O_4@SiO_2 magnetic nanoparticles modified with sodium dodecyl sulfate, a new promising sorbent for fast adsorption/desorption of cationic drugs

Fatemeh Ghanbari Adivi[1] · Payman Hashemi[1] · Abbas Dadkhah Tehrani[1]

Received: 29 July 2017 / Revised: 2 February 2018 / Accepted: 26 June 2018 / Published online: 13 July 2018

Abstract

Agarose-coated Fe_3O_4/SiO_2 magnetic nanoparticles (Fe_3O_4@SiO_2@Agarose) modified with sodium dodecyl sulfate (SDS) were synthesized for adsorption/desorption of cationic drugs applications. For this purpose, magnetic nanoparticles (MNPs) of Fe_3O_4 were synthesized via a chemical precipitation method and the MNPs were homogeneously included into a silica shell using a modified Stöber process. The surface of the core–shell Fe_3O_4@SiO_2 nanoparticles was then modified with SDS and covered with an extra outer shell of agarose. The particles were characterized by X-ray diffraction, scanning electron microscopy, energy-dispersive X-ray analysis, Fourier transform infrared spectroscopy and vibrating-sample magnetometer, differential scanning calorimetry, dynamic light scattering and zeta potential measurements. The applicability of the synthesized nanocomposite for the adsorption/desorption of phenazopyridine (PHP) as a cationic drug model from aqueous solutions was investigated. The effects of different parameters on the adsorption efficiency of PHP such as volume of sample, amount of adsorbent, pH of solution, and contact time were optimized by a central composite design (response surface) method, and effect of volume and type of eluent and desorption time was studied by a one-at-a-time procedure. Under the optimized conditions, a capacity of 41 mg g^{-1} of PHP was obtained for the sorbent with an adsorption efficiency of 92.6% ($\pm$1.5) for 6 replicates. The adsorption isotherms were also studied for the sorbent, and the Freundlich model was found to be more applicable than the Langmuir model in interpreting PHP adsorption on the nanocomposite.

Keywords Fe_3O_4@SiO_2@Agarose sorbent · Sodium dodecyl sulfate · Polymer nanocomposite · Phenazopyridine

✉ Payman Hashemi
Hashemi.p@lu.ac.ir

[1] Department of Chemistry, Faculty of Science, Lorestan University, Khoramabad, Islamic Republic of Iran

Introduction

Polymer nanocomposites containing magnetic iron oxide nanoparticles have attracted considerable attention in recent years. An important reason may be the fact that they often get the desirable characteristics of both organic and inorganic compounds [1–3]. These hybrid materials which contain Fe_3O_4 magnetic nanoparticles (MNPs) are widely used in biomedical and diagnostic fields [4]. The main advantage of these magnetic nanocomposites is their easy separation by an external magnetic field. Despite the magnetic properties of Fe_3O_4 nanoparticles, they need to be coated by different materials to provide conservation against degradation, better biocompatibility and easy surface functionalization. Therefore, providing a suitable coating for iron oxide nanoparticles is essential [5–7]. Many materials have been investigated for modifying the surface of MNPs such as carbon-bimetals [8], noble metals [9], chitosan [1, 2] and silica [10]. Among these, silica offers a combination of properties of biocompatibility, biodegradability and low toxicity. Also, providing binding sites for organic molecules due to the availability of OH groups on the silica surface may further increase its biological applications [1, 2, 11].

Agarose, the purified gelling fraction of agar, is a linear biopolymer and consists of repeating units of alternating b-D- and 3,6-anhydro-a-L-galactopyranosyl groups [12, 13]. It has many useful properties such as being biodegradabe, nontoxic, chemically inert, optically transparent, highly hydrophile, eco-friendly, and biocompatible [14, 15]. Agarose-based adsorbents are well known as excellent support materials for preconcentration and speciation experiments because of their hydrophilicity and chemical resistance in a wide pH range of 0–14 [16, 17].

Phenazopyridine hydrochloride (PHP), with the chemical name of 3-(Phenylazo)-2,6–pyridinediamine hydrochloride (Fig. 1), is a urinary tract anti-pain agent used in oral administrations. It is absorbed in the gastrointestinal region and is mostly excreted from the urine [18, 19]. It is often consumed in combination with sulfonamides and antibiotics, and with an antibacterial agent in order to treat urinary tract infections. In this base, the determination of PHP in biological media, pharmacy and medicines is of great importance [20].

In this paper, a simple and effective method for the synthesis of sodium dodecyl sulfate (SDS) modified agarose-coated $Fe_3O_4@SiO_2$ core/shell nanocomposite is presented. The Fe_3O_4 nanoparticles synthesized by an easy co-precipitation method are coated with SiO_2 via the Stöber method and further modified by SDS and coated

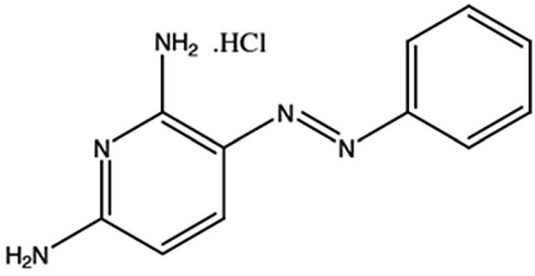

Fig. 1 Structure of phenazopyridine monohydrochloride (PHP)

with an outer shell of agarose to prepare the target nanocomposite. Due to the hydrophilicity and biocompatibility of the polymer-inorganic nanocomposite particles, it is applied as a novel material for the separation, absorption and desorption of PHP as a model compound. The factors influencing the extraction efficiency of PHP are studied using experimental design and response surface methods (RSM).

Materials and methods

Apparatus

UV–visible absorbance spectra were obtained using a Shimadzu 1650PC spectrophotometer. FT-IR spectra were recorded in the range of 4000–400 cm^{-1} by KBr pellet method using a Shimadzu, model 8400 (Japan) spectrometer in the transmittance mode. X-ray diffraction (XRD) patterns were taken using X-ray diffractometer (Panalytical X'Pert Pro, Holland) operating with a Cu anode at 40 kV and 30 mA. A Malvern Zetasizer (ZEN3600, UK) was used for dynamic light scattering (DLS) and zeta potential measurements. The features of Fe_3O_4@SiO_2@Agarose were observed using a field emission scanning electron microscopy (SEM) equipped with energy-dispersive X-ray analysis (EDX) (FE SEM, TESCAN MIRA3 LMU) under an accelerating voltage of 20 kV. The magnetic properties of Fe_3O_4@SiO_2@Agarose were characterized with a vibrating-sample magnetometer (VSM MDKFT, Iran) in a field ranging from −10 to + 10 kOe at room temperature. Differential scanning calorimetry (DSC) analysis was carried out with a DSC1 thermal analysis system (Mettler toledo) under nitrogen atmosphere and a heating rate of 10 °C min^{-1}.

Materials

Tetraethyl orthosilicate (TEOS) and (3-aminopropyl) triethoxysilane (APTES) were purchased from Acros (organic, USA). Iron(II) chloride tetrahydrate ($FeCl_2{\cdot}4H_2O$) was purchased from VWR international (USA). Agarose (medium electroendosmosis for electrophoresis), SDS, iron (III) chloride anhydrous ($FeCl_3$), ethanol (99.9%), aqueous ammonia solution (25 wt%) and other chemicals used in the experiments were obtained from Merck (Darmstadt, Germany) and used without additional purification. Deionized water was used during the experiments. Stock solution (200 mg L^{-1}) of PHP was prepared by dissolving appropriate amount of PHP in deionized water and further diluted daily prior to use. Phosphate buffer solution (0.02 mol L^{-1}) with different pH values was used to adjust solutions pH.

Synthesis of Fe_3O_4 nanoparticles

Fe_3O_4 nanoparticles were synthesized by co-precipitation method as previously reported [21]. The co-precipitation overall reaction is described by the following equation [22]:

$$FeCl_2 + 2FeCl_3 + 8NH_3 + 4H_2O \rightarrow Fe_3O_4 + 8NH_4Cl \quad (1)$$

Briefly, 0.324 g $FeCl_3$ and 0.198 g $FeCl_2{\cdot}4H_2O$ was dissolved in 50 mL of 5% acetic acid solution. The mixture of iron salts was deoxygenated by purging argon and sonicated for 15 min in a thermostated bath at 25 °C. In the next step, this solution was heated to 80 °C and 6 mL of concentrated solution of NH_4OH (25 wt%) was added to it dropwise. The color of solution was changed from yellowish to black, and the reaction mixture was kept at 80 °C for 30 min and then stirred for 1.5 h at 90 °C under argon atmosphere. Subsequently, the synthesized Fe_3O_4 nanoparticles were separated by a permanent magnet and washed with deionized water several times and redispersed to obtain ultrafine magnetic particles.

Preparation of Fe_3O_4@SiO_2

Following the Stöber process with some modifications [1], the prepared magnetic nanoparticles (0.1 g) were dispersed in a mixture of 80 mL ethanol, 16 mL water and 2 mL ammonia solution (25 wt%). The reaction mixture was sonicated for 15 min in a thermostated bath at 25 °C. Then, TEOS (1 mL) and APTES (0.5 mL) were added to the reaction solution with stirring at 25 °C for 18 h. Then, the product was separated and repeatedly washed with ethanol and deionized water.

Synthesis of agarose-coated Fe_3O_4@SiO_2

The above silica-coated nanoparticles were homogenously dispersed in 100 mL solution containing 2.94 g (0.5 mol L^{-1}) NaCl and 720 mg SDS (0.025 mol L^{-1}) for 4 h under magnetic stirring. Then, the prepared nanoparticles were washed with water and the excess SDS in suspension was removed by centrifugating at 6000 rpm for 15 min. The surface-modified particles were then redispersed in 200 mL of 0.2 mol L^{-1} acetate buffer of pH 3.5. A 1% agarose solution was prepared by dissolution of 1.0 g agarose powder in 100 mL boiling water. A volume of 10 mL of the 1% agarose solution was added to the mixture, and it was stirred for 12 h at room temperature. The black product was separated by a permanent magnet and washed three times by a 0.002 mol L^{-1} acetate buffer of pH 3.8 and deionized water. The obtained nanoparticles had a black color, and their sizes were increased several times due to a high water uptake that indicate their coating with agarose. The agarose-coated magnetic Fe_3O_4@SiO_2 particles were stored in water at 4 °C. Schematic illustration of the synthesis procedure of the magnetic agarose-coated nanoparticles is illustrated in Fig. 2.

Adsorption studies

In the present research, a central composite design (CCD) method was used to determine and optimize the effects of four factors on the adsorption efficiency of PHP. Volume of sample, amount of adsorbent, pH of solution and contact time were the four variables included in the design. The low and high levels for each variable were

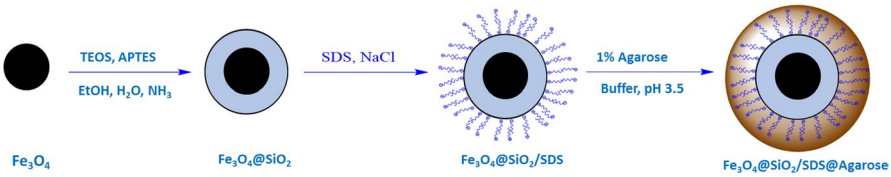

Fig. 2 Schematic illustration of the synthesis procedure of Fe_3O_4@SiO_2@Agarose MNPs

defined according to the results of some early trials. The four studied factors and the five levels designed for each factor by the CCD model are summarized in Table 1. The percent adsorption of the drug was considered as response function during the experiments. In all cases, design initiation and statistical analyses were carried out using the software package, Minitab 16.

Adsorption of PHP from aqueous solutions (10 mg L^{-1}) was studied in a batch system. The pH was adjusted by phosphate buffer solutions (0.02 mol L^{-1}). The solution was shaken at room temperature for a preset time and the PHP loaded Fe_3O_4@SiO_2@Agarose particles were separated from the mixture with a permanent magnet within 5 s. The amount of adsorbed PHP was calculated by difference from the initial PHP concentration and its remaining concentration in the aqueous solution after adsorption using a UV/visible spectrophotometer at the maximum absorbance–wavelength of PHP (340 nm). Standard solutions of PHP were used for the calibration. The percent adsorption, i.e., the drug removal efficiency, was calculated using

$$\%E = \left[\left(C_o - C_t\right)/C_o\right] \tag{2}$$

in which $\%E$ represents the percent adsorption and C_o and C_t represent the initial and final (after adsorption) concentrations of PHP (mg L^{-1}), respectively.

For calculation of the adsorption capacity of the adsorbent, its loading in the presence of different PHP concentrations were measured. For this purpose, 5 mg of the adsorbent was added to 2.5 mL of PHP solutions at pH 8.3 and with different concentrations. The residual amount of the drug in solution was determined spectrophotometrically at 430 nm. The adsorption capacity was calculated from

$$q = \left[\left(C_o - C_t\right) \cdot V\right]/M \tag{3}$$

which q is the amount of analyte adsorbed per unit mass of adsorbent particles representing the adsorption capacity (mg g^{-1}), C_o and C_t represent the initial and

Table 1 Studied factors and levels for the CCD optimization

Factor	Factors' levels				
	Low			High	
pH	7	8	9	10	11
Amount of adsorbent (mL)	0.5	1	1.5	2	2.5
Volume of sample (mL)	2.5	5	7.5	10	12.5
Contact time (min)	2.5	5	7.5	10	12.5

equilibrium concentrations of PHP (mg L^{-1}), V is the volume of the aqueous phase (mL), and M is the mass of adsorbent (mg).

The effects of volume and type of eluent and desorption time were studied by a one-at-a-time procedure. Desorption of drug from the adsorbent was investigated using different kinds of organic solvents (acetonitrile/H_2O, ethanol/H_2O, methanol/H_2O and acetonitrile) in different volumes and times.

Results and discussion

Characterization of MNPs

The FT-IR spectra of the products in each step of the nanoparticles synthesis were recorded to confirm the formation of the expected products. The related spectra are shown in Fig. 3. The characteristic peak of Fe–O at 570 cm^{-1} as seen in Fe_3O_4 spectrum (Fig. 3a) has appeared in the other spectra (Fig. 3b–d) [23]. The bands in the range of 1200–1000 cm^{-1} in (Fig. 3b–d) assigned to the Si–O covalent bond vibrations confirmed the coating of silica on nanoparticles.

The absorption peaks at 3398 and 1542 cm^{-1} in Fe_3O_4@SiO_2 spectrum (Fig. 3b) attributed to the stretching and bending vibrations of amino groups [11] and the absorption bands at 2920 and 2852 cm^{-1} in Fig. 3b can be assigned to C–H groups stretching vibration of the (3-aminopropyl) triethoxysilane (APTES) used to

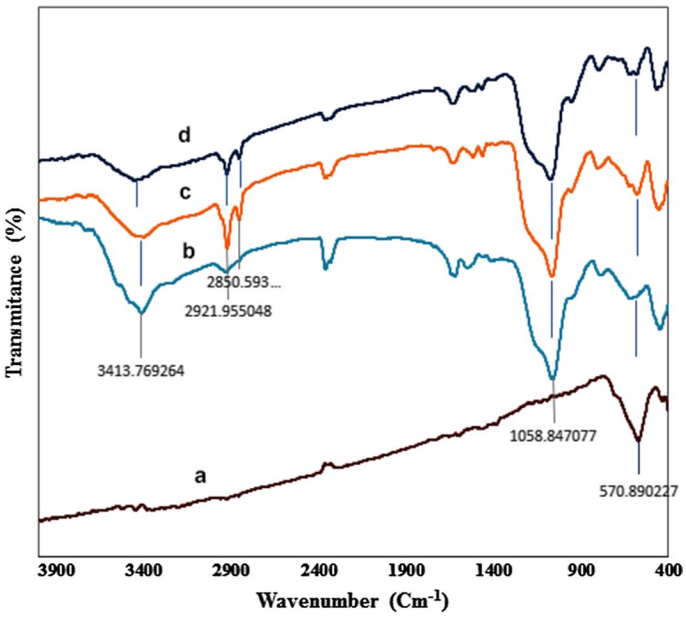

Fig. 3 FT-IR spectra of **a** Fe_3O_4, **b** Fe_3O_4@SiO_2, **c** Fe_3O_4@SiO_2@SDS and **d** Fe_3O_4@SiO_2@Agarose MNPs

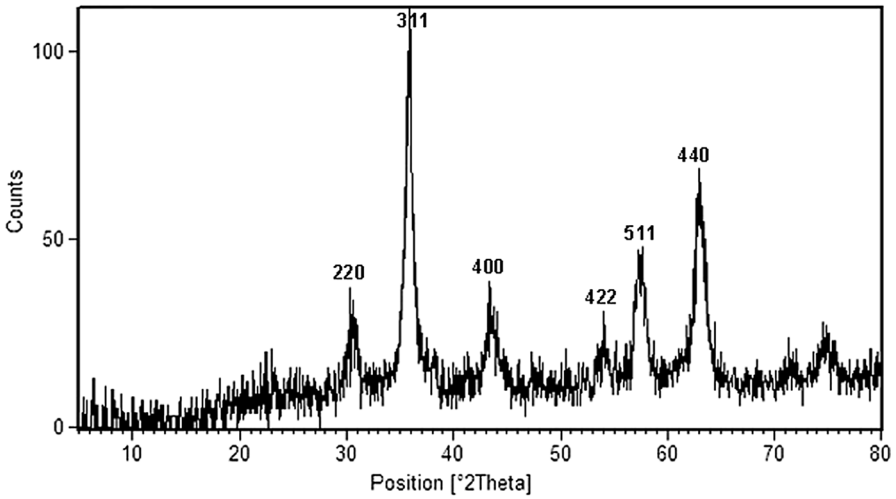

Fig. 4 XRD patterns of Fe_3O_4@SiO_2@Agarose MNPs

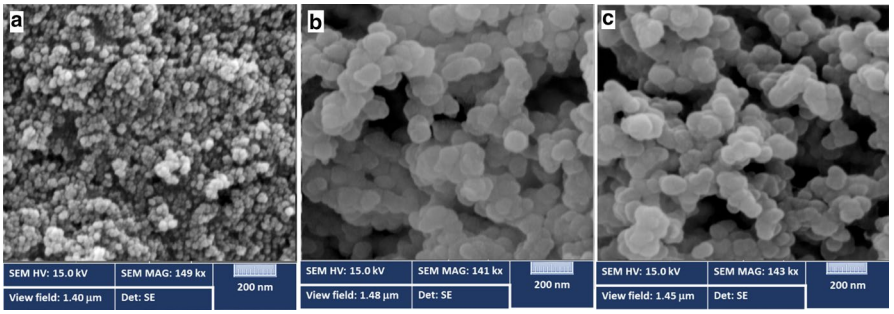

Fig. 5 SEM images of **a** Fe_3O_4, **b** Fe_3O_4@SiO_2, and **c** Fe_3O_4@SiO_2@Agarose MNPs

synthesize Fe_3O_4@SiO_2 and the same peaks in Fig. 3c, d can be assigned to C–H groups of SDS and agarose.

The XRD patterns of Fe_3O_4@SiO_2@Agarose MNPs are shown in Fig. 4. The characteristic peaks at $2\theta = 30.6°$, 35.9°, 43.5°, 54.1°, 57.4°, and 63.0° can be ascribed to crystal planes of (220), (311), (400), (422), (511), and (440) of cubic Fe_3O_4 (JCPDS 19-0629), respectively. This revealed that Fe_3O_4@SiO_2@Agarose nanocomposite did not lead to phase change of Fe_3O_4, while the broad band at $2\theta = 23°–27°$ is assigned to amorphous silica [1]. The XRD results indicated that the Fe_3O_4@SiO_2@Agarose nanocomposite contains the crystalline phases of cubic Fe_3O_4 and silica.

The size and morphology of Fe_3O_4, Fe_3O_4@SiO_2 and Fe_3O_4@SiO_2@Agarose nanocomposites were evaluated by SEM. As seen in Fig. 5, the average size of Fe_3O_4@SiO_2@Agarose was within 50–70 nm with a spherical morphology. EDX analysis and elemental mappings obtained from it were used to measure the atomic

species and elemental distribution present in Fe_3O_4@SiO_2 and Fe_3O_4@SiO_2@Agarose nanocomposites. On the basis of EDX analysis (Table 2), the elements C, O, N, Si and Fe were detected and as expected, the carbon content of Fe_3O_4@SiO_2@Agarose was higher than that of Fe_3O_4@SiO_2 due to the presence of SDS and agarose in the former. Nitrogen was detected in EDX analysis because of the Stöber method used and the use of APTES in the reaction before coating the particles by SDS.

The introduction of NH_2 groups onto the nanoparticles provides the necessary active sites through which SDS and agarose can be further immobilized. The FT-IR, XRD, SEM and EDX analyses clearly confirm the coating of the surface of magnetic nanoparticles of Fe_3O_4 with SiO_2 and agarose shells.

Dynamic Light Scattering (DLS) and zeta potential (ZP) measurements were carried out to determine the size and ZP values of Fe_3O_4@SiO_2@Agarose particles at different pH. The ZP varies with pH and becomes more positive in acidic and more negative in basic pH. In the isoelectric point, which usually denotes also the point of zero charge (PZC), colloids lose stability and agglomeration or flocculation is observed [24]. The values of the mean hydrodynamic diameter, polydispersity index (PDI) and ZP of the Fe_3O_4@SiO_2@Agarose sorbent were measured in two different pHs of 5.5 and 9.0. The ZP of the particles was only -8.26 (± 3.97) mV in pH 5.5, but it was as large as -28.4 (± 5.53) mV in the basic pH of 9.0. In the lower pH, that was close to the isoelectric point, the average size of the particles became larger (1200 nm), probably due to some particle agglomeration. In the basic pH of 9.0, on the other hand, the colloid was more stable in the larger ZP, and a smaller average particle size was observed (398 nm).

Distribution profiles of the hydrodynamic diameters obtained from DLS measurements for Fe_3O_4@SiO_2@Agarose particles at pH 5.5 and 9.0 are presented in Fig. 6. It can be seen that the particle sizes at pH 5.5 (Fig. 6b) are larger than that of the sizes at pH 9.0 (Fig. 6a). The DPI values also showed the same trend and were 0.546 and 0.395 nm in the acidic and basic pHs, respectively.

A comparison with the particle sizes observed in the SEM images (Fig. 5) indicate that the sizes obtained by the DLS method are evidently larger. The reason is that DLS method measures the mean hydrodynamic diameter, which is substantially larger for a nanocomposite with the outer shell of agarose gel in the solution. Furthermore, due to the intensity of the scattered light which increases with increasing the size of objects the mean hydrodynamic diameter obtained by cumulant analysis is overestimated [2].

The magnetic behavior of Fe_3O_4@SiO_2@Agarose at room temperature is shown in Fig. 7 in the form of a magnetization curve with the magnetic field intensity

Table 2 Quantitative results of EDX

Sample type	Element surface compositions determined by EDX (%)				
	C	N	O	Fe	Si
Fe_3O_4@SiO_2	18.1	10.4	53.7	6.4	11.4
Fe_3O_4@SiO_2@Agarose	28.3	10.4	48.1	5.9	7.6

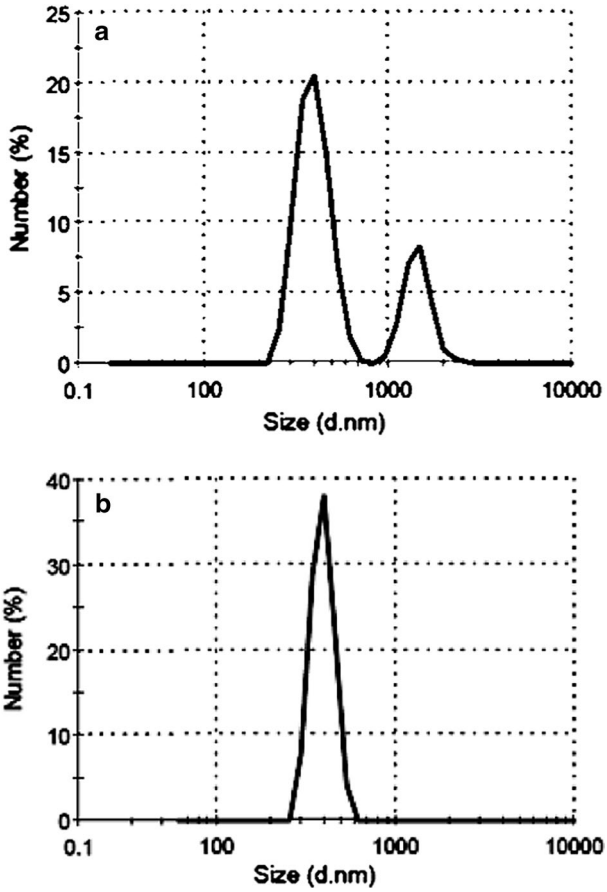

Fig. 6 Distribution profiles of the hydrodynamic diameters obtained from DLS measurements for Fe_3O_4@SiO_2@Agarose particles **a** at pH 5.5 and **b** at pH = 9

variation from + 10,000 to − 10,000 Oe. The saturation magnetization of Fe_3O_4@SiO_2@Agarose nanoparticles is 21.57 emu g^{-1} which is smaller than the values typical of the reference value for the pure magnetite nanoparticles [25]. This reduction of the magnetization which is often observed for nanoparticles may be related to the contribution of the silica and agarose shells surrounding the magnetite nanoparticles. However, the magnitude of this reduction is not so great to seriously affect the applicability of the nanoparticles in magnetic separations. As shown in Fig. 7, the hysteresis loop at 300 K revealed that Fe_3O_4@SiO_2@Agarose displayed low coercivity with no obvious hysteresis confirming the superparamagnetic properties of the nanoparticles [26].

The result of DSC analysis for Fe_3O_4@SiO_2@Agarose is shown in Fig. 8. A DSC curve of Fe_3O_4@SiO_2@Agarose exhibited a broad endothermic peak at around 70 °C which might be due to vaporization of the traces of moisture present. The organic compounds of nanocomposites were decomposed in the temperature range

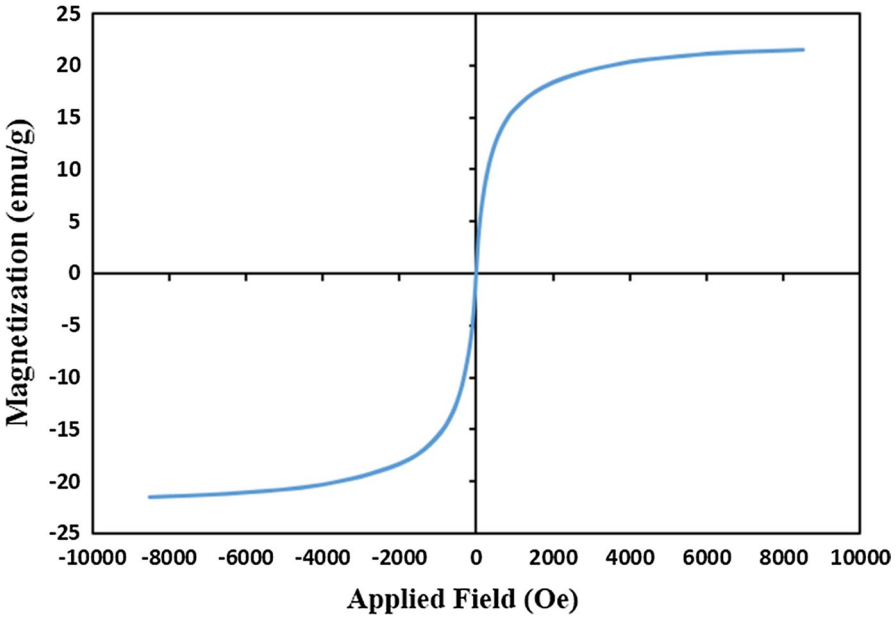

Fig. 7 Magnetization curve of Fe_3O_4@SiO_2@Agarose MNPs

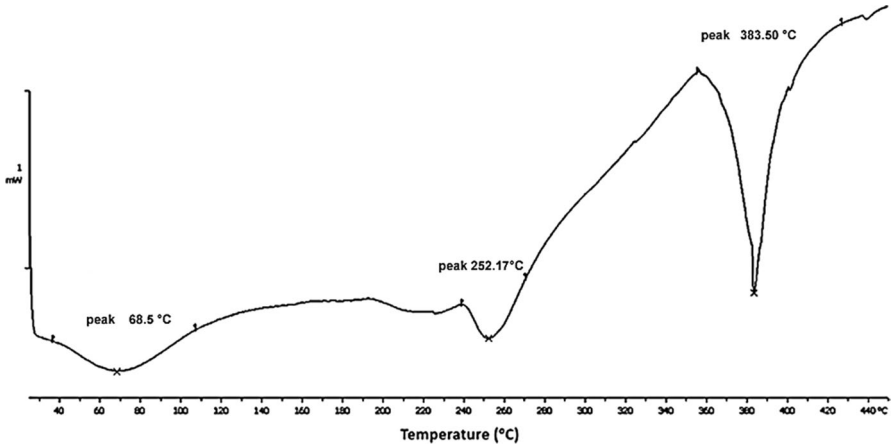

Fig. 8 DSC curve of Fe_3O_4@SiO_2@Agarose MNPs

of 250–600 °C. The strong endothermic peak at 383 °C can be attributed to the degradation of the agarose backbone.

Central composite design (CCD) optimization

One of the most common methods of multivariate optimization is central composite design (CCD) that combines two-level full or fractional factorial designs with additional axial or star points and at least one point at the center of the experimental region being investigated. It allows the determination of both linear and quadratic models [27]. To calculate a good estimate of experimental error (pure error), center points are usually repeated [28].

For optimization of the adsorption parameters, a CCD method was used. Four factors of pH, volume of sample, amount of adsorbent and contact time were included in the design. The low and high levels for each factor were defined according to the results of some preliminary experiments (see Table 1). The percent adsorption of the drug was the dominant criterion that was considered as the response function of the CCD model to optimize the mentioned variables. The levels of the experimental variables designed by the method and the respective response values obtained by performing the experiments are presented in Table 3.

Using the response optimizer function of the Minitab software for simultaneous optimization of the studied factors, the optimization plots were obtained (Fig. 9). An optimization plot indicates how the factors affect the predicted responses. Each column of the graph corresponds to a factor and each cell shows how the corresponding response variable or composite desirability change as a function of one of the factors, while all other factors remain fixed. As shown in Fig. 9c, an increase in adsorption was observed by decreasing the volume of sample and increasing the amount of adsorbent. Also, increasing the pH of solution to 8.3 was resulted in increasing the adsorption (Fig. 9a) but the adsorption efficiency of PHP does not significantly changes with increasing the contact time (Fig. 9d).

Variation of pH can change the surface charge of MNPs [29]. As it is confirmed by the ZP results, in a higher pH value the surface charge of the Fe_3O_4@SiO_2@Agarose particles is more negative. Because of the sorption mechanism, negative surface charges are more proper for the extraction of PHP. This is confirmed by the increase in the adsorption efficiency up to pH 8.3 in Fig. 9a. On the other hand, more basic conditions lead to the prolapse of SDS layer from the nanocomposite and a decrease in adsorption efficiency of PHP is observed.

According to Fig. 9d, the contact time does not have significant effect on the adsorption efficiency of PHP stating a fast adsorption process for the sorbent. The amount of adsorbent and sample volume showed opposite effects on the extraction efficiency of the Fe_3O_4@SiO_2@Agarose sorbent for PHP (Fig. 9b, c). A larger amount of the adsorbent results in a higher collision probability with PHP and provides a higher loading capacity of the sorbent and, as a result, leads to a higher adsorption efficiency. A larger sample volume, on the other hand, shows the opposite effect and decreases the efficiency of adsorption.

Table 3 Conditions of the designed experiments and the respective response values obtained by performing the experiments for central composite design optimization

Run order	pH	Sorbent (mL)	Volume (mL)	Time (min)	Adsorption (%)
1	10	1	10	5	36.92
2	8	1	10	5	35.98
3	9	1.5	7.5	7.5	53.53
4	8	2	5	5	72.40
5	10	2	5	5	71.45
6	9	1.5	7.5	7.5	58.24
7	10	2	10	10	53.34
8	10	1	10	10	33.34
9	8	2	10	5	56.74
10	9	1.5	12.5	7.5	36.36
11	9	1.5	7.5	2.5	57.87
12	8	1	5	10	55.98
13	9	1.5	7.5	7.5	58.43
14	9	1.5	7.5	7.5	55.42
15	9	1.5	2.5	7.5	80.70
16	10	1	5	5	53.90
17	11	1.5	7.5	7.5	27.11
18	8	2	5	10	70.32
19	10	2	10	5	34.47
20	9	0.5	7.5	7.5	26.92
21	10	2	5	10	72.77
22	7	1.5	7.5	7.5	49.00
23	9	1.5	7.5	12.5	49.19
24	9	2.5	7.5	7.5	67.87
25	9	1.5	7.5	7.5	51.64
26	9	1.5	7.5	7.5	53.90
27	8	1	10	10	35.98
28	9	1.5	7.5	7.5	52.58
29	10	1	5	10	53.15
30	8	1	5	5	60.70
31	8	2	10	10	59.00

For the entire data, the predicted optimized conditions calculated from the model were as follows: pH = 8.3, volume of sample = 2.5 mL, amount of adsorbent = 2.5 mL (5 mg) and contact time = 2.5 min. The predicted value for the recovery was 97.89 with an individual desirability of 0.97653. The composite desirability was 0.97653. Performing 6 replicated analyses under the optimized conditions suggested by the CCD model, an adsorption efficiency of 92.6% (± 1.5) was obtained for PHP. Figure 10 shows the images of PHP aqueous

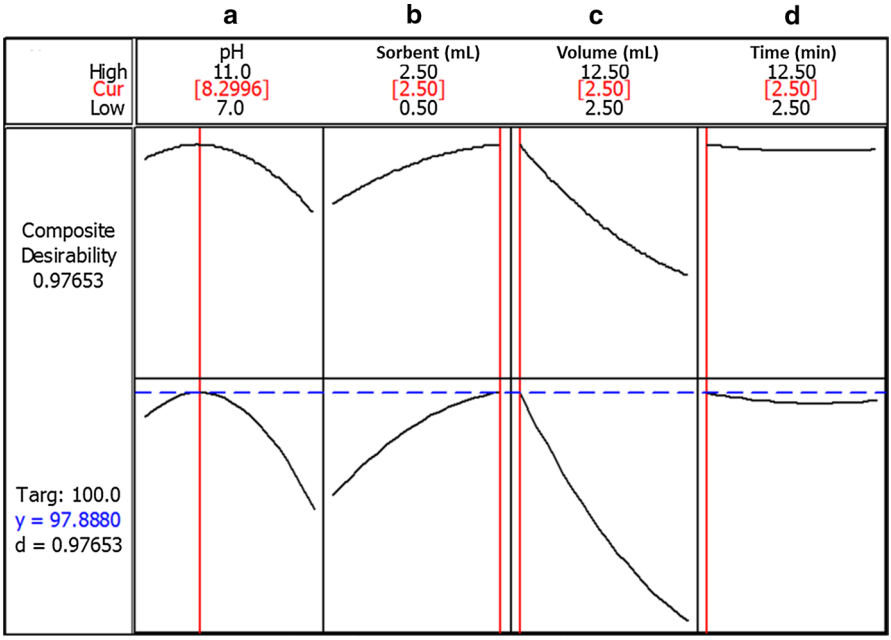

Fig. 9 Simultaneous optimization plots of the studied factors for CCD optimization. **a** pH of solution, **b** amount of adsorbent, **c** volume of sample, **d** contact time

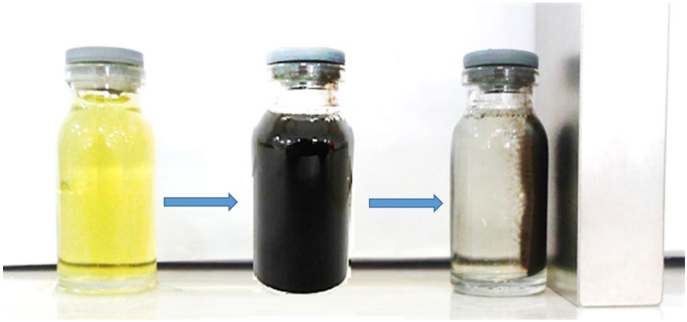

Fig. 10 Images of PHP aqueous solutions before adsorption (left), after addition of the MNPs (center) and after adsorption and magnetic separation of the MNPs by a permanent magnet (right)

solutions before adsorption and after adsorption and magnetic separation of the Fe_3O_4@SiO_2@Agarose particles by a permanent magnet.

Adsorption capacity

The effect of the initial concentration of PHP on the adsorption capacity of the nanocomposite in the optimized conditions is shown in Fig. 11. As can be seen, the adsorption capacity of Fe_3O_4@SiO_2@Agarose nanocomposite increases almost

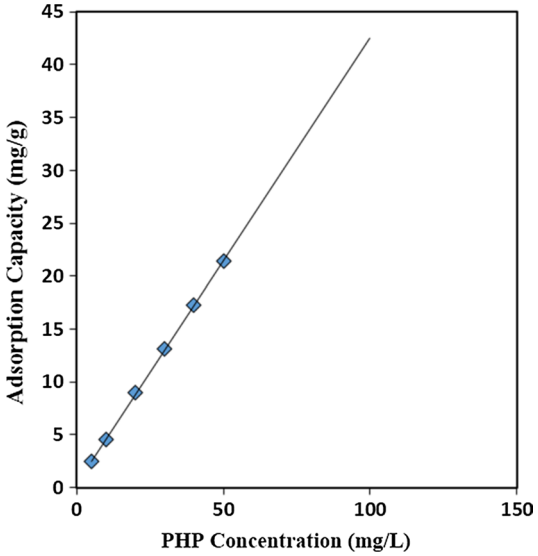

Fig. 11 Effect of the initial concentration of PHP on the adsorption capacity of MNPs under the optimized conditions; pH 8.3; *T* 25 °C, *t* 2.5 min

linearly as the initial concentration of PHP increases. It should be noted that the adsorption profile did not get into a flat region. The maximum PHP adsorption capacity of Fe_3O_4@SiO_2@Agarose for a 100 mg L^{-1} of PHP concentration was 41 mg g^{-1}.

During batch experiments, adsorption isotherms were used to describe the interaction of PHP with the adsorbent. Langmuir and Freundlich isotherms were used to analyze the experimental data. The Langmuir adsorption model is valid for monolayer adsorption onto surface containing fixed number of well-defined sites which can be described by

$$C_e/q_e = 1/bq_m + C_e/q_m \tag{4}$$

in which q_{max} is the maximum adsorption capacity (mg g^{-1}), b is the Langmuir constant (L mg^{-1}), and C_e is the equilibrium PHP concentration in solution (mg L^{-1}). b and q_m are calculated from the slop and intercept of the straight line of the plot of C_e/q versus C_e (Fig. 12a).

The Freundlich isotherm describes reversible adsorption and is not limited to the formation of the monolayer. This empirical equation can be represented by

$$\log q_e = \log k_F + 1/n \log C_e \tag{5}$$

in which k_F and n are the Freundlich constants related to adsorption capacity and adsorption intensity, respectively. k_F and $1/n$ can be obtained from the linear plot of log q versus log C_e (Fig. 12b).

The values of b, q_m, k_F, and n were calculated to be 0.13 L mg^{-1}, 43 mg g^{-1}, 5.14 and 1.4, respectively. Considering R^2 as a measure of the goodness of fit of experimental data [30], the Freundlich model, with an R^2 value of 0.9997, was more applicable than the Langmuir model, with an R^2 of 0.947, in interpreting PHP adsorption on the Fe_3O_4@SiO_2@Agarose MNPs. The better fitting by the Freundlich isotherm

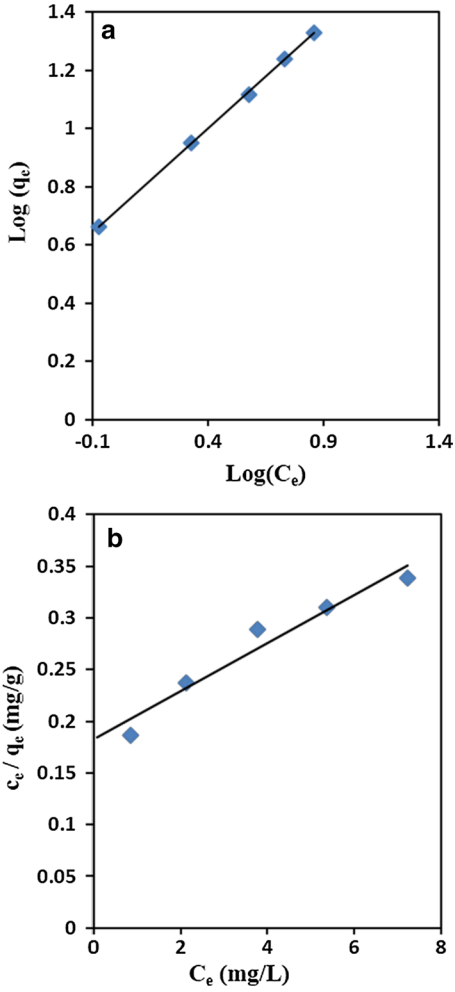

Fig. 12 **a** Langmuir and **b** Freundlich adsorption isotherms for the data of Fig. 11

illustrated the possibility of multilayer adsorption process on the surface of the nanoparticles. The Freundlich constant n is found to be greater than one, representing a suitable condition for the adsorption [31].

Optimization of desorption parameters

Different desorption factors including type and volume of eluent solvent and desorption time were studied. The results are shown in Fig. 13. Mixed solvents with 1:1 volume ratios of methanol/H_2O, ethanol/H_2O, acetonitrile/H_2O, and acetonitrile were investigated as desorption solvents. As shown in Fig. 13a, acetonitrile/H_2O provided the highest desorption efficiency for the Fe_3O_4@SiO_2@Agarose nanocomposite.

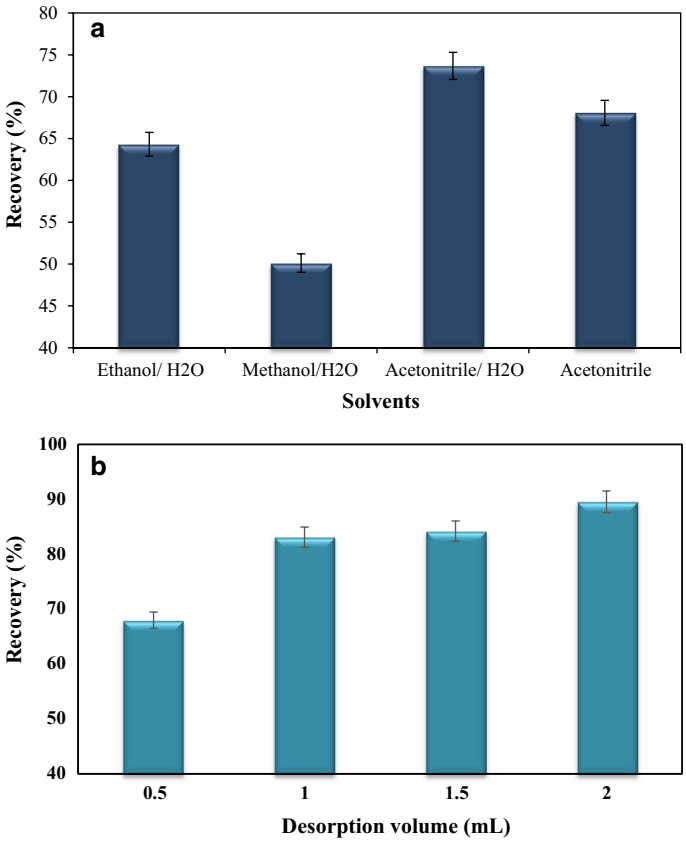

Fig. 13 Effect of different desorption parameters on the extraction efficiency of PHP: **a** type of desorption solvent, **b** volume of desorption solvent

The effect of contact time on the desorption of PHP from the sorbent was investigated in a range of 10–150 s, and no significant difference in the results was observed by increasing the time. However, for safety reasons, 1.0 min was used in subsequent experiments as the optimum desorption time. Figure 13b shows the effect of elution solvent volume on the desorption efficiency of PHP. As can be seen, a volume of 2 mL of acetonitrile/H_2O efficiently desorbs the loaded PHP and may be considered as the optimum volume of the adsorbent. The relatively high volume of acetonitrile/H_2O needed for the desorption of PHP from the sorbent may be attributed to the hydrophilicity and gel character of the agarose layer of Fe_3O_4@SiO_2@Agarose nanocomposite.

Conclusions

In the present study, a novel two-step modifying process for coating Fe_3O_4 nanoparticles with uniform shells of silica, SDS surfactant and hydrogel agarose has been described. Fe_3O_4@SiO_2@Agarose nanoparticles were successfully prepared and characterized in each case by FT-IR, EDX, SEM, XRD, DSC, DLS, ZP and VSM. The synthesized nanocomposite for separation and removal of PHP as drug model was successfully utilized. The modified nanocomposite created a large surface-to-mass ratio and easy usability with high adsorption efficiency for PHP in a short time. The adsorption on the obtained nanocomposite for PHP fitted into Freundlich isotherm. The maximum adsorption capacity for 100 mg L^{-1} of PHP concentration was found to be 41 mg/g. It may be concluded from the results that Fe_3O_4@SiO_2@Agarose as an inorganic–organic hybrid can be potentially applied for the removal of pharmaceutical residues and considering the superparamagnetic properties and the ease of its chemical modification, it may find uses as a novel material in mild separation, enzyme immobilization, etc.

References

1. Lei Z, Pang X, Li N, Lin L, Li Y (2009) A novel two-step modifying process for preparation of chitosan-coated Fe 3 O 4/SiO 2 microspheres. J Mater Process Technol 209:3218–3225
2. Lewandowska-Łańcucka J, Staszewska M, Szuwarzyński M, Kępczyński M, Romek M, Tokarz W, Szpak A, Kania G, Nowakowska M (2014) Synthesis and characterization of the superparamagnetic iron oxide nanoparticles modified with cationic chitosan and coated with silica shell. J Alloys Compd 586:45–51
3. Oh JK, Park JM (2011) Iron oxide-based superparamagnetic polymeric nanomaterials: design, preparation, and biomedical application. Prog Polym Sci 36:168–189
4. Narayanan S, Sathy BN, Mony U, Koyakutty M, Nair SV, Menon D (2011) Biocompatible magnetite/gold nanohybrid contrast agents via green chemistry for MRI and CT bioimaging. ACS Appl Mater Interfaces 4:251–260
5. Rahman M, Nahar Y, Ullah W, Elaissari A, Ahmad H (2015) Incorporation of iron oxide nanoparticles into temperature-responsive poly (N-isopropylacrylamide-co-acrylic acid) P (NIPAAm-AA) polymer hydrogel. J Polym Res 22:1–9
6. Guo J, Yang W, Wang C (2013) Magnetic colloidal supraparticles: design, fabrication and biomedical applications. Adv Mater 25:5196–5214
7. Ahmad H, Kumar K, Rahman M, Rahman M, Miah M, Minami H, Nuri M (2013) Preparation and characterization of conducting polyaniline layered magnetic nano composite polymer particles. Polym Adv Technol 24:740–746
8. An Q, Yu M, Zhang Y, Ma W, Guo J, Wang C (2012) Fe3O4@ carbon microsphere supported Ag–Au bimetallic nanocrystals with the enhanced catalytic activity and selectivity for the reduction of nitroaromatic compounds. J Phys Chem C 116:22432–22440
9. Wang C, Daimon H, Sun S (2009) Dumbbell-like Pt – Fe3O4 nanoparticles and their enhanced catalysis for oxygen reduction reaction. Nano Lett 9:1493–1496
10. Sahoo B, Devi KSP, Dutta S, Maiti TK, Pramanik P, Dhara D (2014) Biocompatible mesoporous silica-coated superparamagnetic manganese ferrite nanoparticles for targeted drug delivery and MR imaging applications. J Colloid Interface Sci 431:31–41
11. Wang J, Zheng S, Shao Y, Liu J, Xu Z, Zhu D (2010) Amino-functionalized Fe 3 O 4@ SiO 2 core–shell magnetic nanomaterial as a novel adsorbent for aqueous heavy metals removal. J Colloid Interface Sci 349:293–299

12. Aymard P, Martin DR, Plucknett K, Foster TJ, Clark AH, Norton IT (2001) Influence of thermal history on the structural and mechanical properties of agarose gels. Biopolymers 59:131–144
13. Fernandez E, Lopez D, Mijangos C, Duskova-Smrckova M, Ilavsky M, Dusek K (2008) Rheological and thermal properties of agarose aqueous solutions and hydrogels. J Polym Sci, Part B: Polym Phys 46:322–328
14. Serenjeh FN, Hashemi P, Rasoolzadeh F (2015) A simple method for the preparation of spherical core–shell nanomagnetic agarose particles. Colloids Surf Physicochem Eng Asp 465:47–53
15. Li J, Guo Z, Zhang S, Wang X (2011) Enrich and seal radionuclides in magnetic agarose microspheres. Chem Eng J 172:892–897
16. Safdarian M, Hashemi P, Adeli M (2013) One-step synthesis of agarose coated magnetic nanoparticles and their application in the solid phase extraction of Pd (II) using a new magnetic field agitation device. Anal Chim Acta 774:44–50
17. Hashemi P, Rahmani Z (2006) A novel homocystine–agarose adsorbent for separation and preconcentration of nickel in table salt and baking soda using factorial design optimization of the experimental conditions. Talanta 68:1677–1682
18. Rao RN, Maurya PK, Raju AN (2009) Isolation and characterization of a potential process related impurity of phenazopyridine HCl by preparative HPLC followed by MS–MS and 2D-NMR spectroscopy. J Pharm Biomed Anal 49:1287–1291
19. Rezaei B, Jafari M, Rahmanian O (2011) Selective pretreatment and determination of phenazopyridine using an imprinted polymer-electrospray ionization ion mobility spectrometry system. Talanta 83:765–769
20. Yagmur S, Yilmaz S, Sadikoglu M, Saglikoglu G, Yildiz M, Yengin C, Kilinc E (2013) Electrooxidation of phenazopyridine hydrochloride and its voltammetric and hplc determination in human urine and tablet dosage form. Int J Electrochem Sci 8:6818–6828
21. Sauzedde F, Elaissari A, Pichot C (1999) Hydrophilic magnetic polymer latexes. 1. Adsorption of magnetic iron oxide nanoparticles onto various cationic latexes. Colloid Polym Sci 277:846–855
22. Gupta AK, Gupta M (2005) Synthesis and surface engineering of iron oxide nanoparticles for biomedical applications. Biomaterials 26:3995–4021
23. Yamaura M, Camilo R, Sampaio L, Macedo M, Nakamura M, Toma H (2004) Preparation and characterization of (3-aminopropyl) triethoxysilane-coated magnetite nanoparticles. J Magn Magn Mater 279:210–217
24. Bhattacharjee S (2016) DLS and zeta potential—what they are and what they are not? J Controlled Release 235:337–351
25. Ni Q, Chen B, Dong S, Tian L, Bai Q (2015) Preparation of core–shell structure Fe3O4@ SiO2 superparamagnetic microspheres immoblized with iminodiacetic acid as immobilized metal ion affinity adsorbents for His-tag protein purification. Biomed Chromatogr 30:566–573
26. Chen L, Berry RM, Tam KC (2014) Synthesis of β-cyclodextrin-modified cellulose nanocrystals (CNCs)@ Fe3O4@ SiO2 superparamagnetic nanorods. ACS Sustain Chem Eng 2:951–958
27. Bezerra MA, Santelli RE, Oliveira EP, Villar LS, Escaleira LA (2008) Response surface methodology (RSM) as a tool for optimization in analytical chemistry. Talanta 76:965–977
28. Serenjeh FN, Hashemi P, Safdarian M, Kheirollahi Z (2014) Semi-automated cloud point extraction with cold column trapping of surfactant-rich phase for phenazopyridine determination in human serum. J Iran Chem Soc 11:733–739
29. Ahalya K, Suriyanarayanan N, Sangeetha S (2014) Effect of pH and annealing temperatures on structural, magnetic, electrical, dielectric and adsorption properties of manganese ferrite nano particles. Mater Sci Semicond Process 27:672–681
30. Al-Asheh S, Banat F, Al-Omari R, Duvnjak Z (2000) Predictions of binary sorption isotherms for the sorption of heavy metals by pine bark using single isotherm data. Chemosphere 41:659–665
31. Ai L, Jiang J (2012) Removal of methylene blue from aqueous solution with self-assembled cylindrical graphene–carbon nanotube hybrid. Chem Eng J 192:156–163